The nonequilibrium mechanism for ultrasensitivity in a biological switch: Sensing by Maxwell's demons

Yuhai Tu*

T. J. Watson Research Center, IBM, P. O. Box 218, Yorktown Heights, NY 10598

Communicated by Charles H. Bennett, IBM Thomas J. Watson Research Center, Yorktown Heights, NY, May 20, 2008 (received for review December 19, 2007)

The *Escherichia coli* flagellar motor senses the intracellular concentration of the response regulator CheY-P and responds by varying the bias between its counterclockwise (CCW) and clockwise (CW) rotational states. The response is ultrasensitive with a large Hill coefficient (≈10). Recently, the detailed distribution functions of the CW and the CCW dwell times have been measured for different CW biases. Based on a general result on the properties of the dwell-time statistics for all equilibrium models, we show that the observed dwell-time statistics imply that the flagellar motor switch operates out of equilibrium, with energy dissipation. We propose a dissipative allosteric model that generates dwell-time statistics consistent with the experimental results. Our model reveals a general nonequilibrium mechanism for ultrasensitivity wherein the switch operates with a small energy expenditure to create high sensitivity. In contrast to the conventional equilibrium models, this mechanism does not require one to assume that CheY-P binds to the CCW and CW states with different affinities. The estimated energy consumption by the flagellar motor switch suggests that the transmembrane proton motive force, which drives the motor's rotation, may also power its switching. The existence of net transitional fluxes between microscopic states of the switch is predicted, measurement of these fluxes can test the nonequilibrium model directly. Both the results on the general properties of the dwell-time statistics and the mechanism for ultrasensitivity should be useful for understanding a diverse class of physical and biological systems.

signal transduction | dissipative system | dwell-time statistics | energy consumption | flagellar motor

High sensitivity has been observed in many signaling systems in biology ranging from calcium signaling in skeletal muscle (1) to chemotaxis response in *Escherichia coli* (2, 3). One of the most studied systems is the flagellar motor switch, where the key component of the switching complex is a ring of around 34 identical FliM proteins (4). The motor switches stochastically between the CCW and the CW states, with a bias affected by the binding of CheY-P to FliM. The conventional picture described the switch by an equilibrium two-state model where the free energies of the two states depend on the CheY-P concentration, and the transition is driven by thermal fluctuation (5, 6). The large Hill coefficient in the motor CheY-P response curve (7) is then explained in terms of cooperative interactions between the FliM molecules. Models falling within this equilibrium framework include the classical Monod–Wyman–Changeux (MWC) allosteric model (8–10) and the Ising-type model (11) with nearest-neighbor interactions. Indeed, cooperative protein interaction has been proposed as a general mechanism for understanding ultrasensitivity in signaling (12). However, most biological complexes, such as the FliM ring, are embedded in and could strongly interact with other components in the system. A fundamental question therefore arises on how good an approximation these equilibrium models are in describing the underlying biological processes. Are there any relevant nonequilibrium effects? If so, how can they be detected and characterized? In this article, we try to address these general questions while also focusing on understanding the mechanism for *E. coli* flagellar motor's ultrasensitive response to CheY-P. Our choice of this particular system is motivated by the recent experimental measurements of detailed single motor switching statistics (13).

Results

Nonexponential Dwell-Time Statistics and the Breakdown of Detailed Balance. The observable state of the flagellar motor is represented by a binary variable s: $s = 0, 1$ corresponds to the CW and CCW rotational states of the motor. The internal state of the switch is described by an integer variable n: $n = 0, 1, 2, \ldots, N$ corresponds to the CheY-P occupancy among the $N(= 34)$ FliM monomers. The stochastic switching kinetics is determined by the transition probability rates between these $2 \times (n + 1)$ states as illustrated in Fig. 1. The CheY-P binding and unbinding rates for a given state (s, n) are $k_s^-(n)$ and $k_s^+(n)$, which depends on the CheY-P concentration $[Y]$. The switching rate from the s state to the $(1 - s)$ state for a given FliM occupancy n is $\omega_s(n)$. Given these transition rates, the steady state probability $p_s^{(0)}(n)$ in state (s, n), the CW (CCW) bias $B_{\rm CW}$ ($B_{\rm CCW}$), and the distribution function $P_s(\tau)$ for dwell time τ in the s state can be determined either by numerical simulation or by solving the master equations (see *Materials and Methods* for details).

For equilibrium systems, detailed balance is satisfied between pairs of states, e.g., $\omega_0(n)p_0^{(0)}(n) = \omega_1(n)p_1^{(0)}(n)$, and, equivalently, the transition rates obey thermodynamic relations, e.g., $k_0^+(n)\omega_0(n+1)k_1^-(n+1)\omega_1(n) = k_0^-(n+1)\omega_1(n+1)k_1^+(n)\omega_0(n)$. By using these relations in analyzing the master equations for $P_s(\tau)$, we discover that the dwell-time distribution function can be expressed as a sum of exponential decay functions with positive definite coefficients [see supporting information (SI) *Text* for details of the proof]:

$$P_s(\tau) = \sum_{j=0}^{N} c_j \exp(-\lambda_j \tau), \quad \lambda_j > 0, \quad c_j \geq 0. \qquad [1]$$

We emphasize that this result is valid for any equilibrium model with detailed balance, including the Ising-type model (see *SI Text* and Fig. S1 for details). From Eq. **1**, $P_s(\tau)$ satisfies a set of constraints:

$$(-1)^m \frac{d^m P_s(\tau)}{d\tau^m} > 0, \quad \forall\, \tau > 0, \quad m = 1, 2, 3, \ldots, \qquad [2]$$

in particular, it should be monotonically decreasing ($m = 1$) and convex ($m = 2$). For nonequilibrium systems, some of the

Author contributions: Y.T. designed research, performed research, analyzed data, and wrote the paper.

The author declares no conflict of interest.

*E-mail: yuhai@us.ibm.com.

This article contains supporting information online at www.pnas.org/cgi/content/full/0804641105/DCSupplemental.

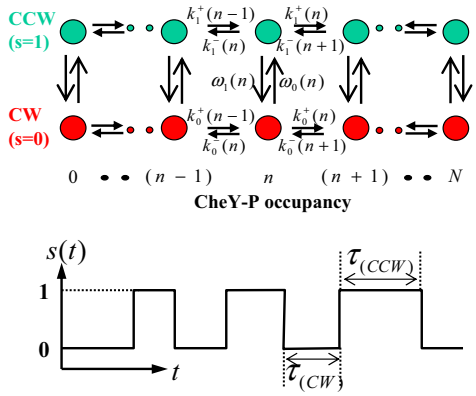

Fig. 1. Illustration of the general kinetic model for flagellar motor switching in the state space spanned by two state variables *s* and *n*, which represent the rotational state and the CheY-P occupancy of the switch, respectively. A stochastic switching time series is shown for the observable state variable *s*(*t*).

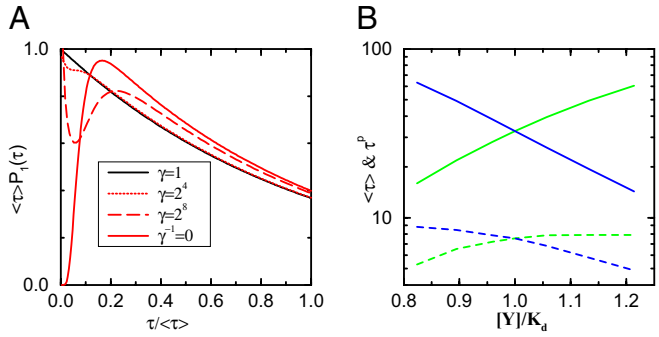

Fig. 2. The behaviors of the dwell-time distribution and its dependence on γ and [*Y*]. (*A*) System starting from being exponential for the equilibrium model (black line) with $\gamma = 1$, $P_1(\tau)$ shows progressively stronger nonequilibrium signatures as γ increases: concavity for $\gamma = 16$ (dotted red line), nonmonotonicity for $\gamma = 256, \infty$ (dashed and solid red lines). The solid red line is for the limit γ arrow ∞ and $\bar{\omega}$ arrow 0 with $\bar{\omega}\,\gamma = 12.8$, which corresponds to the unidirectional case where at least one of the transitional rates $\omega_0(n)$ or $\omega_1(n)$ is zero for any given *n*: $\omega_0(n)\omega_1(n) = 0$. Only in this unidirectional case, $P_1(\tau)$ vanishes at $\tau = 0$. All of the curves correspond to $[Y]/K_d = 1$ (or $B_{CW} = 0.5$), other parameters used here are $n_L = 12$, $n_U = 22$, $C = 1$, $\bar{\omega} = 0.05$ (except for the solid red line). (*B*)The average dwell time $\langle\tau\rangle$ (solid lines) and the peak time τ^p dotted lines) versus CheY-P concentration [*Y*] from our model with $\gamma = 256$ and other parameters the same as in *A*, the CCW state (blue lines) and the CW state (green lines) show opposite dependence on [*Y*].

coefficients c_j can become negative and consequently some of the constraints for $P_s(\tau)$ can be violated.

This general property of the dwell-time statistics provides a powerful tool in identifying possible nonequilibrium effects. Violation of any constraints in Eq. **2** is sufficient (but not necessary) to imply breakdown of detailed balance in the underlying kinetics. For the *E. coli* flagellar motor, detailed statistics of the single motor switching kinetics were measured recently by the Cluzel laboratory (13), for a series of given CW biases and at a higher resolution than previous experiments (14). The distribution functions of the CW and CCW dwell times are found to have a distinctive peak at a finite value. The accuracy of the measured $P_s(\tau)$ for small τ can be affected by experimental resolution as well as ambiguity in defining the CCW and CW states when the system is in the transitional states. However, the switching between CCW and CW states is extremely fast, occurring on the millisecond time scale (15); therefore, the observed peaks in $P_s(\tau)$ at times of up to 0.4 sec (13) are experimentally very well resolved. According to our general theory on dwell-time statistics, the presence of such peaks in $P_s(\tau)$ clearly indicates that the flagellar motor switch operates out of equilibrium. Thus, we suggest that the conventional models of flagellar motor switching need to be modified in a fundamental way to reflect the breakdown of thermodynamic relations and the violation of detailed balance.

Dissipative Allosteric Model and the Nonequilibrium Mechanism for High Sensitivity. To capture the nonequilibrium nature of the switching kinetics, we modify the equilibrium transition rates $\omega_s^{(e)}(n)$ by a factor $\gamma_s(n)$: $\omega_s(n) = \gamma_s(n)\omega_s^{(e)}(n)$ with $\gamma_0(n) \neq \gamma_1(n)$. $k_BT\ \ln(\gamma_0(n))$ and $k_BT\ \ln(\gamma_1(n))$ can be interpreted as the decreases of the energy barrier from the CW and CCW sides of the double-well potential respectively (k_B is the Boltzmann constant, T is the absolute temperature). The equilibrium model corresponds to the special case when $\gamma_0(n) = \gamma_1(n)$ for all n.

For this article, $\omega_s^{(e)}(n)$ are taken to be the same as in the equilibrium MWC allosteric model (8) with two dissociation constants $K_{d,0}$ and $K_{d,1}$ for CheY-P binding to FliM in the CW and CCW states, respectively. The general behavior of the dissipative allosteric model is studied with the simple choice of constant $\gamma_{0,1}(n)$ in separate regions of n: $\gamma_1(n \geq n_U) = \gamma$, $\gamma_1(n < n_U) = 1$; $\gamma_0(n \leq n_L) = \gamma$, $\gamma_0(n > n_L) = 1$ with $n_U \geq n_L$. Other choices of $\gamma_{0,1}(n)$, such as exponential dependence $\gamma_0(n) = \gamma_1(N - n) = b^{N/2-n}$ with $b > 1$, do not change the qualitative behaviors of the model (see Fig. S2 for results for other choices of $\gamma_{0,1}(n)$ studied). The dwell-time statistics and the sensitivity of the switch are determined by solving the master equations for different model parameters. In Fig. 2*A*, we show the changes of the CCW dwell-time distribution functions $P_1(\tau)$ as γ increases. For $\gamma = 1$ (the equilibrium model), $P_1(\tau)$ follows an exponential-like distribution. As γ increases, nonequilibrium characteristics, such as concavity and nonmonotonicity, develop progressively in $P_1(\tau)$ as predicted from our theory. As shown in Fig. 2*B*, the average dwell time $\langle\tau\rangle$ and the dwell time τ^p at the peak of the dwell-time distribution function for the CCW (CW) state decrease (increase) with the CheY-P concentration, in qualitative agreement with the experimental observation (13).

The most important function of the flagellar motor switch is its ultrasensitive response to CheY-P. For the equilibrium model ($\gamma = 1$), the response to CheY-P is driven by the difference in CheY-P-binding affinities to the CCW and the CW states, i.e., $C \equiv K_{d,0}/K_{d,1} < 1$. Quantitatively, a Hill coefficient of 10 in the equilibrium models requires a more than 4-fold difference in CheY-P binding ($C \leq 0.25$). Despite much effort, this has not been observed (16). In contrast, for the nonequilibrium model even when CheY-P binds equally to FliM in CCW and CW states ($C = 1$), highly sensitive response to CheY-P develops for large values of γ as shown in Fig. 3*A*. The sensing of CheY-P in the nonequilibrium model depends on the two amplification factors $\gamma_0(n)$ and $\gamma_1(n)$. Intuitively, these two nonequilibrium factors can be understood as resulting from the actions of two Maxwell demons (17, 18). In the context of our model, the two demons operate to irreversibly enhance the CW → CCW or CCW → CW transition rates beyond their equilibrium values in different regions of the switch's CheY-P occupancy state space ($n \leq n_L$ or $n \geq n_U$, respectively). Their opposing actions with different dependence on CheY-P level give rise to the dependence of the switch's CW bias on CheY-P concentration. Effectively, the two demons act as the switch's sensors for the CheY-P concentration. A highly sensitive switch can be made, provided γ is large, and the operation regions for the two opposing demons are well separated (large $\Delta n \equiv n_U - n_L$).

The second law of thermodynamics prescribes that the Maxwell demons consume energy to carry out their work, i.e., to sense and respond to CheY-P. The rate of energy consumption $\dot{W}$ can be calculated from our model (19, 20):

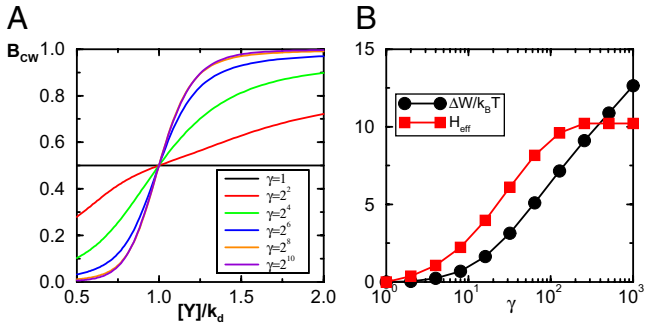

Fig. 3. The response curves and the energy dissipation. (*A*) The response curves for different values of $\gamma = 1,2^2,2^4,2^6,2^8,2^{10}$, with $C = 1$ and other parameters $\bar{\omega} = 0.01$, $n_U = 22$, $n_L = 12$. The black line ($\gamma = 1$) corresponds to the equilibrium case with a constant response (zero sensitivity) for $C = 1$. (*B*)The effective Hill coefficient H_{eff} (red line) of the response curves in *A* and the energy dissipation $\Delta W/k_BT$ (black line) are plotted for different γ values on a semilog plot.

$$\dot{W} = k_B T \sum_{\langle AB \rangle} (J_{AB} - J_{BA}) \ln\left(\frac{J_{AB}}{J_{BA}}\right), \qquad [3]$$

where the sum is over all pairs of states $\langle$AB$\rangle$, J_{AB} is the probability flux from state A to state B. The net flux from A to B: $\Delta J_{AB} \equiv J_{AB} - J_{BA}$ is nonzero only in nonequilibrium systems because of the breakdown of detailed balance. In fact, measurements of this net flux can be used to directly test the validity of the nonequilibrium models (see *SI Text* for a detailed calculation of these fluxes). The average energy dissipated per switch cycle (CCW to CW to CCW) is $\Delta W = (\tau_1 + \tau_0)\dot{W}$, where τ_0 and τ_1 are the average dwell time for CW and CCW states, respectively. In Fig. 3*B*, the energy dissipation $\Delta W/k_BT$ and the Hill coefficient of the corresponding response curve $H_{eff} \equiv 2 \times d(\ln B_{CW})/d(\ln[Y])|_{B_{CW}} = 0.5$ for given values of γ are plotted together. Our result clearly shows that in our nonequilibrium model, sensitivity is powered by energy dissipation, and more energy is needed to generate higher sensitivity (H_{eff}). Eventually, H_{eff} is limited by the size of the operation range Δn, as shown in Fig. 4, where H_{eff} is plotted versus the energy dissipation $\Delta W/k_BT$ for different values of Δn.

Despite the different origins of the equilibrium ($\gamma = 1$, $C < 1$) and the nonequilibrium ($\gamma > 1$) mechanisms for high sensitivity, they can coexist as shown in Fig. 5*A*, where H_{eff} is shown for different values of C and ΔW (by varying γ). For a given C, H_{eff} increases from its equilibrium value at $\Delta W = 0$ ($\gamma = 1$) as the energy dissipation ΔW increases. However, although both

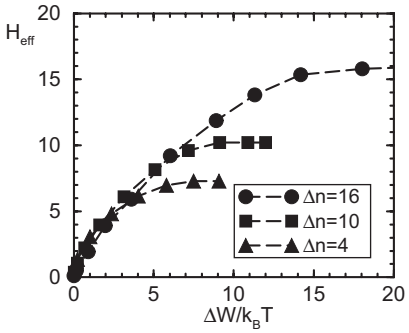

Fig. 4. The dependence of the Hill coefficient H_{eff} on the energy dissipation for three different sizes of the operation gap $\Delta n = n_U - n_L$: $n_L = 15$, $n_U = 19$ (triangle); $n_L = 12$,$n_U = 22$ (square); $n_L = 9$,$n_U = 25$ (circle). Other parameters are the same as in Fig. 3.

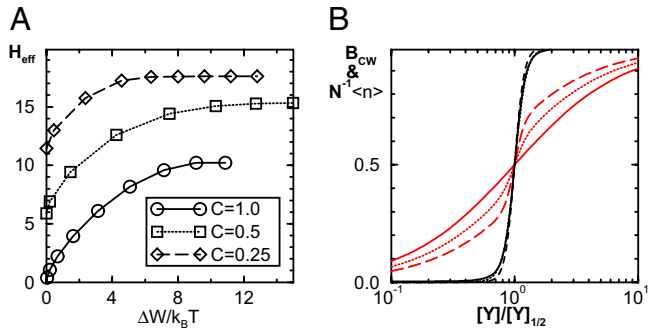

Fig. 5. Comparison of the equilibrium and nonequilibrium models. (*A*) The effective Hill coefficient H_{eff} versus the energy dissipation $\Delta W/K_BT$ for different values of binding affinity ratio: $C = 1.0$ (black line), $C = 0.5$ (red line), and $C = 0.25$ (blue line), other parameters being the same as in Fig. 3. The equilibrium cases correspond to $\Delta W = 0$. (*B*) Almost indistinguishable response curves (black lines) with high sensitivity $H_{teff} = 10$ can be achieved for different values of C with different levels of energy dissipation (or γ), but the behaviors of the average fractional FliM occupancy $N^{-1}\langle n\rangle$ (red lines) are very different. Three cases with parameters $(C,\gamma) = (1, 256),(0.5,16),(0.25,1)$ are plotted as the solid, the dotted, and the dashed lines, respectively.

mechanisms can generate high sensitivity (black lines in Fig. 5*B*), their predicted dependence of average FliM occupancy $\langle n\rangle$ on CheY-P concentration differs significantly. The CheY-P occupancy curve for the equilibrium model ($C = 0.25$, $\gamma = 1$) has a steep region in the operating range of the CheY-P concentration, whereas the FliM occupancy for the nonequilibrium model ($C = 1$, $\gamma = 256$) follows a gradual binding function $\frac{[Y]}{[Y] + [Y]_{1/2}}$ for all CheY-P concentrations, as shown in Fig. 5*B* (red lines). Therefore, careful measurement of FliM occupancy is critical to distinguish between these two mechanisms. The other significant difference between the two mechanisms is their opposite dependence between the switching frequency and sensitivity. We find that increasing γ (>1) in the nonequilibrium model not only increases the sensitivity (H_{eff}), it also increase the switching frequencies $\tau_{0,1}^{-1}$. On the contrary, for the equilibrium models, higher sensitivity (with smaller C) leads to slower switching rates (11) akin to the well known phenomenon of critical slowing down for equilibrium systems.

Discussion

The general theory on the properties of the dwell-time distribution obtained in this article holds true for all equilibrium systems with detailed balance. This theory provides a powerful tool in detecting relevant nonequilibrium effects in all systems and should be particularly useful in biology, where most interesting systems operate out of equilibrium. The nonequilibrium characteristics in the dwell-time distribution function, such as nonmonotonicity (peak), concavity, and other higher-order behaviors, generally appear at time scales much smaller than the average dwell time. Therefore, high-resolution experiments are required to unravel these subtle but highly informative features. Depending on the strength of the nonequilibrium effects, extra care may also be needed to control the signal to prevent weakening of these features by averaging over different signal strengths. For example in the case of the *E. coli* flagellar motor switch, peaks in $P_s(\tau)$ became visible only when $P_s(\tau)$ were determined for fixed CW biases (13). There is a recent report of a similar peak in dwell-time distribution in the kinesin motor for its waiting-time (between steps) distribution at low ATP concentration (21); it would be interesting to study the implication of these observations in light of our work. The strong connection between the dwell-time statistic and the underlying kinetics established here will hopefully stimulate more such careful

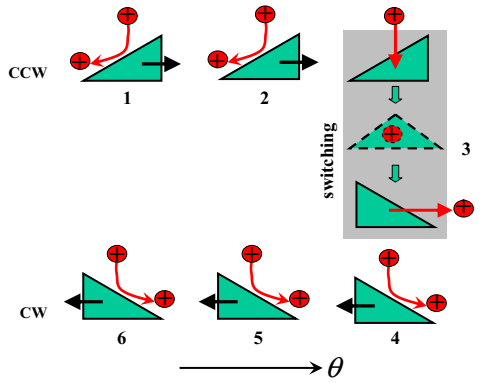

Fig. 6. Illustration of the proposed dual roles of the proton flux. In addition to drive the motion of the motor (time frames 1 and 2 for CCW; time frames 4–6 for CW), each passage of proton (red circle) through the cell membrane may also, with a small probability, drive the switching between CCW and CW states of the motor (time frame 3, the gray box).

measurements of $P_s(\tau)$, particularly for small dwell times, for motors as well as other biological systems.

For the *E. coli* flagellar motor, the nonequilibrium effects are not only necessary in explaining the observed dwell-time statistics; more importantly, they provide a mechanism by which the system dissipates a small amount of energy to produce a highly sensitive, fast response to the signal (CheY-P). To generate the observed high sensitivity for a single flagellar motor, the amount of energy per switch cycle (CCW–CW–CCW) dissipated is in the range of 7–12 k_BT for a variety of detailed models (see Fig. 4 and Fig. S3). Interestingly, this small switching energy is roughly equal to the work done by one to two protons moving through a membrane potential of −170 mV at room temperature, so the energy source for the switch could be the same proton gradient that drives the flagellar motor rotation. Therefore, in addition to the spontaneous switching (controlled solely by CheY-P level), we propose a proton-assisted switching mechanism. The energy released by each proton passage through the membrane, instead of always being converted to mechanical motion, may also (with a small probability) be used in carrying out switching as illustrated in Fig. 6. The probability of this proton-assisted switching can depend on the internal state of the switch, i.e., its rotational sense (CW or CCW) and the CheY-P occupancy of the FliM, this dependence being described by $\gamma_{0,1}(n)$ in our model. The existence of this proton-assisted switching is supported by the important observation by Fahrner, Ryu, and Berg (22) that the average switching frequency depends on the rotational speed of the motor or, equivalently, the proton flux. Molecularly, the FliM ring can tap into the proton energy source through its coupling to the FliG ring (23, 24), which interacts directly with the stator (MotA/MotB) complex, where protons pass through the membrane. Detailed information on these interactions (FliM/FliG/MotAB/proton, etc.) is needed to elucidate the molecular (energy-consuming) switching kinetics. Quantitative switching statistics, such as those measured in ref. 13 but with different loads and proton motive forces, will help determine the quantitative forms of $\gamma_{0,1}(n)$ in our model, their dependence on the proton flux, and the molecular origin of these Maxwell demons. However, independently of the molecular details, our study here clearly demonstrate that the flagellar switch does not operate as an equilibrium apparatus isolated from the rest of the motor as previously conceived. The general nonequilibrium model framework proposed here provides a crucial step toward understanding the switch as a part of the integrated motor system.

One important general feature of the nonequilibrium mechanism for high sensitivity is that it does not require different binding affinities of the signaling molecule to the two different states of the switch, in contrast to the classical equilibrium allosteric mechanism. The measurement of the ligand-binding curve for a single motor in CCW and CW state can therefore be used to distinguish between these two mechanisms. Our nonequilibrium model also predicts the existence of nonzero net transitional fluxes between any pair of microscopic states of the switch; *in vivo* CheY-P/FliM-binding measurements together with the motor switching measurements for the same single motor can be used to measure the net transitional fluxes and test microscopically whether detailed balance is violated in the switching kinetics. Besides the flagellar motor, we speculate that this more robust [details of $\gamma_{0,1}(n)$ do not matter] nonequilibrium mechanism for creating highly sensitive switches with a small energy expenditure may be preferred by a large class of cellular processes to an equilibrium mechanism that requires fine tuning of the binding affinity ratio and the allosteric interaction strength (11). Many signaling systems, especially those with allosteric interactions, such as Ca signaling for cardiac filament activation (25) and signal transduction by MCP chemoreceptor clusters (3, 26–28), should be reexamined in light of the nonequilibrium model developed here.

Materials and Methods

Master Equations for Determining the Dwell-Time Distribution Functions. The master equation for the probability $p_s(n,t)$ of being in state (s, n) at time t is

$$\frac{dp_s(n,t)}{dt} = (1-\delta_{n0})k_s^+(n-1)p_s(n-1,t) + (1-\delta_{nN})k_s^- (n+1)p_s(n+1,t) - (k_s^+(n)+k_s^-(n))p_s(n,t) - \omega_s(n)p_s(n,t) + \omega_{1-s}(n)p_{1-s}(n,t), \quad [4]$$

where $s = 0, 1$ and $n = 0, 1, 2, \ldots, N$. The steady-state distribution $p_s^{(0)}(n)$ is obtained by setting the right hand side of Eq. **4** to 0. The CW bias B_{CW} is derived from $^{(0)}_{s}((n)$:

$$B_{CW} = \frac{\sum_{n=0}^{N} p_0^{(0)}(n)}{\sum_{n=0}^{N}(p_0^{(0)}(n)+p_1^{(0)}(n))}.$$

To obtain the dwell-time distribution functions for CW and CCW, assume that the motor switches from the $(1-s)$ state to the s state at time $t = 0$, and define $Q_s(n,\tau)$ as the subsequent "survival" probability that the motor is still in the s state with n occupied FliM at time $t = \tau > 0$. The master equation for $Q_s(n,\tau)$ is

$$\frac{dQ_s(n,\tau)}{d\tau} = (1-\delta_{n0})k_s^+(n-1)Q_s(n-1,\tau) + (1-\delta_{nN}) k_s^-(n+1)Q_s(n+1,\tau) - (k_s^+(n)+k_s^-(n))Q_s(n,\tau) - \omega_s(n)Q_s(n,\tau), \quad [5]$$

$s = 0,1$. The survival probability $Q_s(n,\tau)$ can be solved from the above equation with the initial condition determined by the steady-state distribution of the $(1-s)$ state: $Q_s(n,\tau=0) = A_s\omega_{1-s}(n)p_{1-s}^{(0)}(n)$, where A_s is normalization factor $A_s = (\sum_{n=0}^{N}\omega_{1-s}(n)p_{1-s}^{(0)}(n))^{-1}$.

Eqs. **4** and **5** are solved by using standard linear algebra and eigenvalue/eigenvector analysis for any given choices of model parameters. Finally, from $Q_s(n,\tau)$, the distribution function for dwell time τ can be obtained:

$$P_s(\tau) = -\sum_{n=0}^{N}\frac{dQ_s(n,\tau)}{d\tau} = \sum_{n=0}^{N}\omega_s Q_s(n,\tau). \quad [6]$$

Details of the Kinetic MWC Model. The equilibrium part of the dissipative allosteric model studied here is the same as the Monod–Wyman–Changeux

(MWC) model (8). Following the energetic representation of the MWC model (29), the free energy (in units of k_BT) for state (s, n) is given by

$$G_s(n) = -\ln\left(\frac{N!}{n!(N-n)!}\right) - [\ln([Y]/K_{d,0}) + s\ln C]n + E_s,$$

where E is the energy difference between the CCW and CW states when $n = 0$. We set $E = N/2\ln C$, known to be optimum in generating high sensitivity (11, 29). The free energy $G_m(n)$ for the intermediate state is chosen in this article to have the same simple dependence on n and $[Y]$:

$$G_m(n) = -\ln\left(\frac{N!}{n!(N-n)!}\right) - [\ln([Y]/K_{d,0}) + A_m\ln C]n + B_mE,$$

where A_m, B_m are constants, chosen to be $A_m = \frac{1}{2}$, $B_m = \frac{1}{2}$ in this article. The equilibrium switching rate $\omega_s^{(e)}(n) = \bar{\omega}\exp(-\Delta G_s)$ depends on the free-energy difference: $\Delta G_s(n) \equiv -G_s(n) + G_m(n)$, where mac$]\omega$ is the (geometrical) average of all these equilibrium rates given the way we choose the intermediate-state free energy. For independent CheY-P/FliM binding (30), we have: $k_s^+(n) = (N-n)k_s^{on}$, $k_s^-(n) = nk_s$off, where $k_{0,1}^{off}$ are the on and off rates for individual CheY-P to FliM binding in the CW and CCW states. These rates are related to the dissociation constants $K_{d,s}$ and the CheY-P concentration $[Y]$: $k_s^{on}/k_s^{off} = [Y]/K_{d,s}$ We let the off rates be $k_s^{off} = 1$ (for both CCW and CW) to set the (fast) time scale for our model. We also let the dissociation constant for CW be $K_{d,0} = 1$ to set the scale for CheY-P concentration $[Y]$. The variable parameters for the equilibrium part of the model studied in this article are $\bar{\omega} \ll 1$ and $C \leq 1$.

Net Transition Fluxes and Energy Dissipation in the Dissipative MWC Model. One distinctive feature of a nonequilibrium system is the existence of a nonzero net transition flux $\Delta J_{AB} \neq 0$ from state A to state B in the system because of breakdown of detailed balance. Quantitatively, the net flux from state (s, n) to state (s, $n+1$) is:

$$\Delta J_s^{(h)}(n) = k_s^+(n)p_s^{(0)}(n) - k_s^-(n+1)p_s^{(0)}(n+1),\ 0 \leq n \leq (N-1).$$

The net CCW to CW switching flux (Fig. S4) from state (1, n) to state (0, n) is:

$$\Delta J_i^{(\nu)}(n) = \omega_1(n)p_1^{(0)}(n) - \omega_0(n)p_0^{(0)}(n),\ 0 \leq n \leq N,$$

the net flux from CW to CCW is just the opposite: $\Delta J_0^{(\nu)}(n) = -\Delta J_1^{(\nu)}(n)$. The total energy dissipated in the system can be decomposed into terms for each link in the transitional network. For the links between states (s, n) and (s, $n+1$), the energy dissipation rate is

$$\delta\dot{\omega}_s^{(h)}(n) = k_BT\Delta J_s^{(h)}(n)\ln\left(\frac{k_s^+(n)p_s^{(0)}(n)}{k_s^-(n+1)p_s^{(0)}(n+1)}\right),\quad 0 \leq n \leq (N-1),$$

whereas for links between states (1, n) and (0, n), the energy dissipation rate is

$$\delta\dot{\omega}^{(\nu)}(n) = k_BT\Delta J_1^{(\nu)}(n)\ln\left(\frac{\omega_1(n)p_1^{(0)}(n)}{\omega_0(n)p_0^{(0)}r(n)}\right),\ 0 \leq n \leq N.$$

Summing over all of the links in the system, we obtain the energy dissipation rate for the whole system: $\dot{W} = \Sigma_{s,n}\delta\, w_s^{(h)}(n) + \Sigma_n\delta\, w^{(\nu)}(n)$.

ACKNOWLEDGMENTS. I thank Drs. G. Grinstein, J. Rice, and G. Stolovitzky for helpful discussions and Dr. Klaus Schwarz for careful reading of the manuscript. This work was partially supported by National Science Foundation Grant CCF-0635134.

1. Bremel RD, Weber A (1972) Cooperation within actin filaments in vertebrate skeletal muscle. *Nat New Biol* 238:97–101.
2. Segall JE, Block SM, Berg, HC (1983) Temporal comparisons in bacterial chemotaxis. *Proc Natl Acad Sci USA* 31:8987–8991.
3. Bray D, Levin MD, Morton-Firth CJ (1998) Receptors clustering as a cellular mechanism to control sensitivity. *Nature* 393:85–88.
4. Berg HC (2003) The rotary motor of bacterial flagella. *Annu Rev Biochem* 72:19–54.
5. Khan S, Macnab RM (1980) The steady state counterclockwise/clockwise ratio of bacterial flagella motors is regulated by prontomotive force. *J Mol Biol* 138:563–597.
6. Scharf BE, Fahrner KA, Turner L, Berg HC (1998) Control of direction of flagellar rotation in bacterial chemotaxis. *Proc Natl Acad Sci USA* 95:201–206.
7. Cluzel P, Surette M, Leibler S (2000) An ultrasensitive bacterial motor revealed by monitoring signaling proteins in single cells. *Science* 287:1652–1655.
8. Monod J, Wyman J, Changeux JP (1965) On the nature of allosteric transitions: a plausible model. *J Mol Biol* 12:88–118.
9. Alon U, *et al.* (1998) Response regulator output in bacterical chemotaxis. *EMBO J* 17:4238–4248.
10. Turner L, Sameul ADT, Stern AS, Berg H (1999) Temerature dependence of switching of the baterial fagella motor by the protein CheY(13DK106YW). *Biophys J* 77:597–603.
11. Duke TAJ, Novere NL, Bray D (2001) Conformational spread in a ring of proteins: A stochastic approach to allostery. *J Mol Biol* 308:541–553.
12. Bray D, Duke T (2004) Conformational spread: The propagation of allosteric states in large multiprotein complexes. *Annu Rev Biophys Biomol Struct* 33:53–73.
13. Korobkova E, Emonet T, Park H, Cluzel P (2006) Hidden stochastic nature of a single bacterial motor. *Phys Rev Lett* 96:058105–058108.
14. Block SM, Segall JE, Berg HC (1983) Adaptation kinetics in bacterial chemotaxis. *J Bacteriol* 154:312–323.
15. Kudo S, Magariyama Y, Aizawa SI (1990) Abrupt changes in flagellar rotation observed by laser dark field microscopy. *Nature* 346:677–680.
16. Sourjik V, Berg HC (2002) Binding of the *E. coli* response regulator CheY to its target is measured in vivo by fluorescence resonance energy transfer. *Proc Natl Acad Sci USA* 99:12669–12674.
17. Maxwell JC (2001) *Theory of Heat* [Longmans Green, London (1871), republished by Dover, New York].
18. Landauer R (1961) Irreversibility and heat generation in the computing process. *IBM J Res Dev* 5:183.
19. Hill TL (1977) *Free Energy Transduction in Biology* (Academic, New York).
20. Hong Q (2006) Open-system nonequilibrium steady state: Statistical thermodynamics, fluctuations, and chemical oscillations. *J Phys Chem B* 110:15063–15074.
21. Mori T, Vale RD, Tomishige M (2007) How kinesin waits between steps. *Nature* 450:750–754.
22. Fahrner K, Ryu WS, Berg HC (2003) Bacterial flagellar switching under load. *Nature* 423:938.
23. Park SY, Lowder B, Bilwes AM, Blair DF, Crane BR (2006) Structure of FliM provides insight into assembly of the switch complex in the bacterial flagella motor. *Proc Natl Acad Sci USA* 103:11886–11891.
24. Brown PN, Terrazas M, Paul K, Blair DF (2007) Mutational analysis of the flagellar protein FliG: Sites of interaction with flim and implecations for organization of the switch complex. *J Bacteriol* 189:305–312.
25. Rice JJ, Stolovitzky G, Tu Y, de Tombey PP (2003) Ising model of cardiac thin filament activation with nearest-neighbor cooperative interactions. *Biophys J* 84:897–909.
26. Duke TAJ, Bray D (1999) Heightened sensitivity of a lattice of membrane of receptors. *Proc Natl Acad Sci USA* 96:10104–10108.
27. Mello BA, Tu Y (2003) Quantitative modeling of sensitivity in bacterial chemotaxis: The role of coupling among different chemoreceptor species. *Proc Natl Acad Sci USA* 100:8223–8228.
28. Sourjik V, Berg HC (2004) Functional interactions between receptors in bacterial chemotaxis. *Nature* 428:s437–s441.
29. Mello BA, Tu Y (2005) An allosteric model for heterogeneous receptor complexes: Understanding bacterial chemotaxis response to multiple stimuli. *Proc Natl Acad Sci USA* 102:17354–17359.
30. Sagi Y, Khan S, Eisenbach M (2003) Binding of the chemotaxis response regulator chey to the isolated, intact switch complex of the bacterial flagellar motor. *J Biol Chem* 278:25867–25871.